International Journal of Automotive Technology, Vol. 22, No. 5, pp. 1279–1290 (2021)
DOI 10.1007/s12239–021–0112–5

pISSN 1229–9138/ eISSN 1976–3832

LIGHTWEIGHT DESIGN OF AN AUTOMOTIVE BATTERY-PACK ENCLOSURE VIA ADVANCED HIGH-STRENGTH STEELS AND SIZE OPTIMIZATION

Yongjun Pan[1)*], Yue Xiong[1)], Lei Wu[2)], Keshan Diao[2)] and Wei Guo[3)]

[1)]State Key Laboratory of Mechanical Transmission, College of Mechanical and Vehicle Engineering, Chongqing University, Chongqing 400044, China
[2)]Technology Center, HBIS Group Tangsteel Company, No.9 Binhe Road, Hebei 063016, China
[3)]School of Automotive Engineering, Wuhan University of Technology, Hubei 430070, China

(Received 10 April 2020; Revised 31 August 2020; Accepted 4 January 2021)

ABSTRACT–The battery packs are crucial components of electric vehicles and may severely affect the continue voyage course and vehicle safety. Therefore, design optimization of the battery-pack enclosure (BPE) is critical for enhanced mechanical and crashwrothiness performances. In this study, a lightweight design of an automotive BPE under the loading conditions is presented based on the advanced high-strength steels (AHSSs) and size optimization. A numerical analysis procedure is also introduced for the lightweight design. First of all, a nonlinear finite element (FE) BPE model was established and validated through the modal test. Secondly, the random vibration simulation was performed based on the sensitivity analysis to initially determine the AHSSs and thickness for the components of the BPE. Next, the material and thickness were determined by the fixed-frequency vibration analysis. Moreover, the mechanical shock and fatigue life were analyzed numerically. Finally, the crashworthiness of the optimized BPE model was verified by crash and crush simulations. The results show that the optimized BPE structure has a 10.41 % lightweight gain, while assuring enhanced dynamic performances. The introduced numerical procedure could be used to quickly determine the material and thickness of each component of BPE. The design optimization process was found beneficial to reduce the number of physical tests and product development cost and shorten product development cycles.

KEY WORDS : Lightweight design, Size optimization, Battery-pack enclosure (BPE), Crashworthiness, Electric vehicle

NOMENCLATURE

FE	: finite element
RMS	: root mean square
BPE	: battery-pack enclosure
FEM	: finite element method
PSD	: power spectral density
CFRP	: carbon fibre reinforced plastics
AHSSs	: advanced high-strength steels

1. INTRODUCTION

In recent years, increasing attention has been paid to serious environmental problems and depleting non-renewable resources because of their continuous consumption. New energy vehicles have been upgraded to the national strategies as an alternative to alleviate energy pressure and reduce environmental pollution. The electric vehicles, as a typical new-energy vehicle with the advantages of zero emissions and high efficiency have gradually become an essential development direction of major automobile companies in the world. The lightweight design of electric vehicles and critical components under various operating conditions has become the focus of current research (Chen *et al.*, 2017b; Liu *et al.*, 2016; Liu *et al.*, 2019; Obradovic *et al.*, 2012).

The battery-pack system, which is one of the crucial components of electric vehicles, directly affects the vehicle safety performance. Currently, these systems are generally large in size and volume, affecting the continue voyage course of electric vehicles. The lightweight design can ensure larger capacity battery packs on the premise of the same weight and improve the continue voyage course of electric vehicles. Improving the energy density of the battery packs has been a difficult task; therefore, the enclosure design should be optimized in terms of weight such as lightweight characteristic to enhance its mechanical and dynamic performances (Arora *et al.*, 2016; Li *et al.*, 2018; Uerlich *et al.*, 2020).

**Corresponding author*. e-mail: yongjun.pan@cqu.edu.cn

2. LITERATURE REVIEW

Over the past decade, a significant effort has been focused on the optimization and lightweight design of battery-pack systems. Hartman *et al.* optimized a battery-pack design to improve its natural frequencies. The new design increased the stiffness of the battery pack and reduced its weight by 20 % (Hartmann *et al*., 2013). Kaleg optimized the design based on aluminum material and found the 2 mm aluminum 5052-0 material as optimum for battery-pack enclosure (BPE), reducing its mass by 6.51 kg (Kaleg, 2016). Wang *et al*. presented a multi-objective topology optimization method to achieve a new BPE structure with enhanced static and dynamic performances (Wang *et al.*, 2016). Lin *et al*., provided a multi-objective optimization procedure for a BPE using metamodel technique and particle-swarm-optimization algorithm to minimize the total mass and maximize the restrained basic frequency (Lin *et al.*, 2016). Chen *et al*., presented a lightweight design of a multi-material BPE, using carbon fibre reinforced plastics (CFRP) as the battery case and aluminum alloy material as the frame structure (Chen *et al.*, 2017a). Schludi and Joos indicated that fiber composite material can be used for BPE. This material has advantages of low weight meeting all safety, stiffness, and thermal management demands (Schludi and Joos, 2019). Pal *et al*. proposed a cold spray technology to improve the mechanical performances of the BPE, including maximizing the minimum natural frequency and minimizing the maximum deformation (Pal *et al.*, 2020).

Advanced high-strength steels (AHSSs) have been increasingly used owing to their advantages of reduced total cost compared to other materials such as aluminum alloys and CFRP. Lightweight BPE can alternatively be obtained using AHSSs (Chen and Zhao, 2019; Chen *et al.*, 2019).

In this study, lightweight BPE design was achieved using AHSS and size optimization, taking account of the detailed enclosure structure. The lightweight design considers materials and thickness optimization under the random vibration analysis, the fixed-frequency vibration analysis, the mechanical shock analysis, and the fatigue life analysis. Further, the crashworthiness performance of the optimized enclosure was verified by crush and crash simulations based on the standard test (Ministry of Industry and Information Technology of the People's Republic of China, 2020). The presented numerical analysis procedure could be used to quickly determine the material and thickness of each component of the BPE for meeting lightweight design and enhanced dynamic performance.

3. MATHEMATICAL MODEL

3.1. Finite Element (FE) Model

Finite element method (FEM) was used to generate detailed distributions of stress and strain of a BPE under the vibration, the mechanical shock, and the crashworthiness. The physical and geometrical features of actual objects should be described accurately for better reliability of the results calculated by the FEM. The basic idea was to discretize continuous geometry into finite elements and set finite nodes so that the continuous structure can be recognized as a set of elements connected only at nodes. In order to control and reduce errors, the FE model should meet performance indicators such as reliability, accuracy, and robustness. The governing partial differential equations of the FE model were derived by the virtual power method or principle of minimum potential energy (Zienkiewicz *et al*., 2014):

$$\boldsymbol{M}\ddot{\boldsymbol{q}}(t) + \boldsymbol{C}\dot{\boldsymbol{q}}(t) + \boldsymbol{K}\boldsymbol{q}(t) = \boldsymbol{F}(t) \tag{1}$$

where matrix $\boldsymbol{M}$ represents the mass matrix of the FE model, matrix $\boldsymbol{C}$ and $\boldsymbol{K}$ represent the stiffness and damping matrices, respectively, and terms $\boldsymbol{q}(t)$ and $\boldsymbol{F}(t)$ contain the nodal displacements and applied forces, respectively.

Figure 1 shows the structure of the BPE investigated in this study.

The BPE contains an upper and a lower enclosure fixed and sealed by screws and sealing. The lower enclosure has a complicated structure containing a bracket, a crossbeam, a

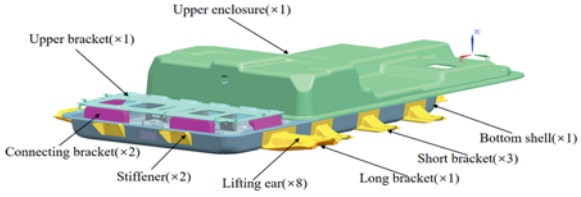

Figure 1. Structure of the BPE.

Table 1. Original materials.

Component	Material	Thickness (mm)
Upper bracket	Carbon steel DC01	1.6
Lifting ear	Carbon steel DC01	2.5
Bottom shell	Carbon steel B280	1
Lower support crossbeam	Carbon steel DC01	1.5
Crossbeam	Carbon steel DC01	1.8
Connecting bracket	Carbon steel B340	2.5
Short bracket	Carbon steel DC01	1.8
Long bracket	Carbon steel DC01	2
Lower support stringer	Carbon steel DC01	2
Stringer	Carbon steel B280	1.8

Table 2. Material properties.

Material	Yield strength (MPa)	Tensile strength (MPa)	Elastic modulus (GPa)	Poisson ratio	Density (kg/mm^3)
Carbon steel DC01	130-260	270-410	207	0.3	7.85×10^{-6}
Carbon steel B210	210-310	≥390	206	0.25-0.3	7.90×10^{-6}
Carbon steel B280	280-420	≥440	206	0.25-0.3	7.90×10^{-6}
Carbon steel B340	340-420	410-510	206	0.25-0.3	7.90×10^{-6}
Carbon steel 06Cr19Ni10	≥205	≥520	206	0.25-0.3	7.93×10^{-6}
Aluminum YL112	165	320	70	0.33	2.74×10^{-6}
Plastic SMC	80-120	135-250	8	0.3	1.85×10^{-6}

bottom shell, connecting brackets, stiffeners, an accompanied circuitry, and a heating and cooling system.

The materials used for the components are mainly DC01, B210, B280, and B340. The upper enclosure is made from carbon-fiber reinforced plastic to provide lighter weight, as it bears little external forces and shocks. The materials used for the main components are shown in Tables 1 and 2.

The thickness of each component ranges from 1 mm to 3 mm, and its aspect ratio is much larger than the thickness. Thus, the BPE can be modeled using the shell element. For the battery packs, a homogenization model was used, because the centralized mass model will increase the frequency error. Figure 2 shows the FE model of the BPE after the geometric cleanup.

If the nodal displacements $\boldsymbol{q}(t)$ that are the so-called primary variables are determined, the structural deformation, the strain and the stress, which are the secondary variables, can be easily calculated by the following equations:

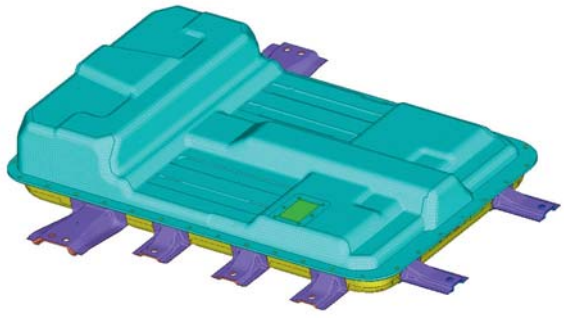

Figure 2. FE model of the BPE.

$$\boldsymbol{u}(x,y,t) = \boldsymbol{N}(x,y)\boldsymbol{q}(t) \tag{2}$$

$$\boldsymbol{\varepsilon}(x,y,t) = \boldsymbol{B}(x,y)\boldsymbol{q}(t) \tag{3}$$

$$\boldsymbol{\sigma}(x,y,t) = \boldsymbol{D}\varepsilon = \boldsymbol{DB}(x,y)\boldsymbol{q}(t) = \boldsymbol{S}(x,y)\boldsymbol{q}(t) \tag{4}$$

where for 2D finite elements, the elastic matrix D can be expressed by the following expression:

$$\boldsymbol{D} = \frac{E}{1-\mu^2}\begin{bmatrix} 1 & \mu & 0 \\ \mu & 1 & 0 \\ 0 & 0 & \frac{1-\mu}{2} \end{bmatrix} \tag{5}$$

3.2. Model Verification and Validation

The model verification in FE analysis is one of the necessary processes, guaranteeing the credibility and validity of the numerical results. Model verification and validation ensure that the model meets intended requirements in terms of the methods used and the obtained results, indicating that in the applicable range, the FE model can support subsequent analysis and have satisfactory calculation accuracy.

The credibility of the FE model was ensured by performing some preliminary checks such as whether the material attributes are correctly assigned, the boundary constraints are properly defined, and the overall geometric model and related elements are accurate. Moreover, parameters such as warpage, internal angle, Jacobi, and aspect ratio of the grid also need to be adjusted and optimized to guarantee the accuracy of the FE model. Through the computer-aided accuracy check, 99.9 % finite elements were qualified. The FE model contained 90679 2D elements, 87141 of which were quadrilateral elements (96.1 %) and 3538 were triangular elements (3.9 %).

When a high quality FE model is established, some simple dynamic analysis should be conducted to ensure the mathematical accuracy of the model. In this section, the numerical results of the constrained modal analysis will be compared to the bench test to verify the effectiveness and validity of the established FE model. The modal analysis can predict the structures' main modal characteristics of each order in a certain frequency range that may be affected. The actual vibration response of the structure under the effects of external or internal vibration sources in the frequency band was predicted by the modal analysis. In the modal simulation, the boundary conditions need to be imposed based on the actual installation to reflect the most realistic results. The BPE was fixed to the chassis by bolts, thus the mounting holes at both ends of the BPE bracket need to be fixed. By performing the constrained modal analysis, the corresponding natural frequencies were obtained as 31.2, 42.0, 44.5, 55.9, 62.1, and 64.9 Hz. The

Table 3. Natural frequencies and modes of vibrations.

Order	Frequency (Hz)	Mode description
1	31.2	Local vibration at the tail of the upper cover and the tail of the bottom shell
2	42	Local vibration in the middle of the upper cover
3	44.5	Local vibration in the middle of the bottom shell
4	55.9	Local vibration in the middle of the upper cover
5	62.1	Local vibration of upper cover and upper bracket
6	64.9	Local vibration between the upper cover and the upper bracket

natural frequencies and modes of vibrations are listed in Table 3.

The first-order natural frequency was measured as 32 Hz by the bench test. The difference between the numerical and test results was approximately 2.5 %, which is acceptable for most of engineering problems, verifying the validity of the nonlinear FE model. Therefore, this FE model could be used for the further dynamic simulations.

4. AHSSS THICKNESS DESIGN

Random Vibration Analysis for Preliminary Design

The vibrations from the acceleration, deceleration, and the road environment will transfer to the vehicles and will inevitably affect the components on the chassis, such as battery packs and enclosure. The vibration simulation can simulate the vibration environment during the actual driving period and analyze the stress and strain of components to provide a reference for the design of vehicle components (Hong *et al.*, 2014; Lang and Kjell, 2015).

The Z-axis random vibration of the BPE is the most severe case, and will be analyzed by the FE model to initially identify the materials and thickness of the enclosure components. Further, the fixed-frequency vibration analysis, the mechanical analysis, and the fatigue life analysis were carried out to optimize the materials and thickness selection. Finally, the crashworthiness performance of the optimized BPE was verified by crush and crash simulations. The entire analysis procedure is shown in Figure 3.

The frequency responses of the BPE was determined based on the random vibration analysis. The standard deviation of the displacement and stress can be obtained, providing a basis to investigate the durability of the BPE. In this section, the random excitation applied to the BPE referred to the test standard. The power spectral density is shown in Table 4. The random vibration test time was optimized by the test stress collection verification, simulation analysis, and feasibility analysis and found as 12 h based on the equivalent damage theory (Ministry of Industry and Information Technology of the People's Republic of China, 2020).

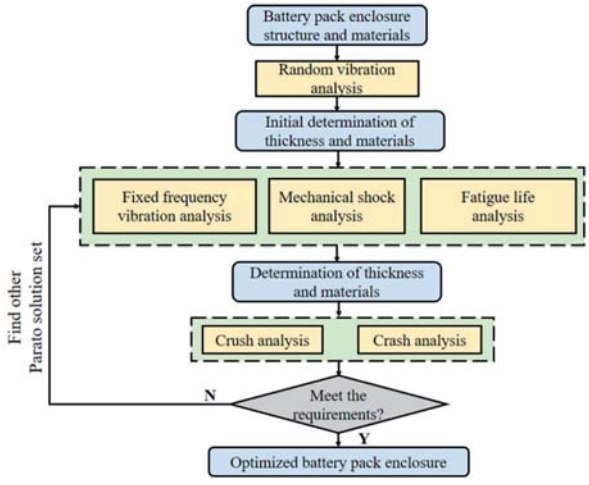

Figure 3. Analysis procedure of BPE.

Table 4. Parameters for random vibration.

Frequency (Hz)	PSD in Z-axis	PSD in Y-axis	PSD in X-axis
5	0.015	0.002	0.006
10	/	0.005	/
15	0.015	/	/
20	/	0.005	/
30	/	/	0.006
65	0.001	/	/
100	0.001	/	/
200	0.0001	0.00015	0.00003
Root mean square (RMS)	0.64 g	0.45 g	0.50 g

Table 5. Material properties.

Material	Yield strength (MPa)	Tensile strength (MPa)	Elastic modulus (GPa)	Poisson ratio	Density (kg/mm^3)
590 DP	398	≥590	210	0.3	7.83×10^{-6}
780 DP	550	≥790	210	0.3	7.83×10^{-6}
980 DP	784	≥980	216	0.28	7.80×10^{-6}

The materials used in the original BPE are DC01, B210, B280, and B340. Among them, DC01 and B280 account for the largest proportion. Only these two materials will be replaced by AHSSs. Further, the thickness of the related components will be optimized based on the sensitivity analysis for the lightweight design. The investigated AHSSs are the dual-phase steels 590 DP, 780 DP, and 980 DP and their properties are shown in Table 5.

The preliminary random vibration analysis indicated that the upper bracket had the highest stress, and its RMS value exceeded 200 MPa. Considering the design requirement of 3 Sigma, only 980 DP material met its strength requirement. The thickness of the upper bracket was 0.2 mm less than the original thickness according to the FE analysis. The materials of other components and their thickness were initially determined based on the random vibration analysis. The simulation process shows that the thickness of each component significantly affected its own stress, but had limited effects on other components; therefore, the thickness sensitivity analysis was performed and the results are shown in Figure 4.

Figure 4 (a) shows the stress of the components when the material DC01 is replaced by material 780 DP. More specifically, 780 DP was used as the material of the lower support crossbeam and lifting ear, while original materials were used for other components. These observation shows that the stresses of the lower support crossbeam and lifting ears vary gradually, while those of the other components approximately remain the same.

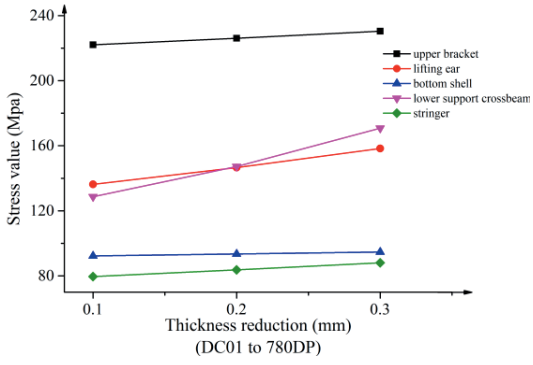

(a) Material selection: DC01 to 780 DP

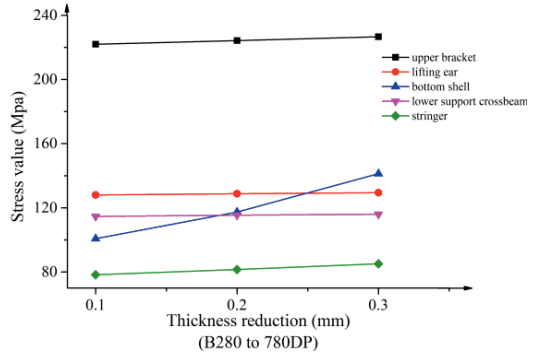

(b) Material selection: B280 to 780 DP

Figure 4. Thickness sensitivity.

Table 6. Initial materials and thickness.

Component	Material	Selection 1 (mm)	Selection 2 (mm)
Upper bracket	980 DP	1.4	1.4
Lifting ear	780 DP	2.3	2.2
Bottom shell	780 DP	0.8	0.8
Lower support crossbeam	780 DP	1.3	1.2
Crossbeam	780 DP	1.6	1.5
Connecting bracket	B340	2.5	2.5
Short bracket	780 DP	1.6	1.5
Long bracket	780 DP	1.8	1.7
Lower support stringer	780 DP	1.3	1.2
Stringer	B210	1.8	1.8

Figure 4 (b) shows the stress of the components when the material B280 is replaced by 780 DP. More specifically, 780 DP was used as the material of the bottom shell, while the original materials were used for the other components. Clearly, the stress of the bottom shell varies gradually, while those of the other components approximately does not show obvious change, providing a basis for the materials and thickness design.

The remaining components were analyzed by the similar procedure. The initially determined materials and thickness are listed in Table 6.

4.1. Fixed-frequency Vibration Analysis

The vibration signals of the washboard road and other roads are not the same type. It has obvious forced vibration characteristics. The energy is concentrated in a very small frequency band. The washboard road has been regarded as a typical pavement and needs to be considered and tested. It is treated according to sine constant frequency based on the data from numerous road spectrum collection. The frequency and test time of the fixed frequency test were simultaneously obtained according to the data analysis of the washboard road at the test site.

The road test and bench test are highly expensive, and the cycle is particularly long. Computer-aided simulations can provide a supplemental and economic approach to evaluate the fixed-frequency vibration performance. In this section, the FEM was used to simulate the constant amplitude vibration test in the bench test, i.e., the fixed-frequency vibration test to compute the stress of each

Table 7. Parameters for fixed-frequency vibration.

Item	Z-axis	Y-axis	X-axis
Fixed-frequency amplitude	±1.5 g	±1.0 g	±1.0 g
Fixed-frequency	24 Hz	24 Hz	24 Hz
Duration	1 h	1 h	1 h

Table 8. Maximum stress of components.

Component	Material	Thick-ness 1 (mm)	Maxi-mum stress (MPa)	Thick-ness 2 (mm)	Maxi-mum stress (MPa)
Upper bracket	980 DP	1.4	444.1	1.4	389.8
Lifting ear	780 DP	2.3	288.6	2.2	448.9
Bottom shell	780 DP	0.8	339.9	0.8	395
Lower support crossbeam	780 DP	1.3	170.5	1.2	417.3
Crossbeam	780 DP	1.6	213.9	1.5	404.6
Connec-tingbracket	B340	2.5	86.9	2.5	86.4
Short bracket	780 DP	1.6	185.4	1.5	341.5
Long bracket	780 DP	1.8	354.4	1.7	361.4
Lower support stringer	780 DP	1.3	591.1	1.2	1153.1
Stringer	B210	1.8	204.9	1.8	338.9

component. The parameters of the fixed-frequency vibration analysis according to the test standard are shown in Table 7.

In the fixed-frequency vibration analysis, the Z-axis faces the most severe stress. Thus, the thickness was initially determined by the random vibration analysis and the numerical results are shown in Table 8.

Table 8 shows that the maximum stress (1153.1 MPa) occurs at the lower support stringer. Thus, the first thickness section was selected for use, because the maximum stress (591.1 MPa) is lower. The thickness of the lower support stringer returned to the original value without any thinning.

In a similar way, the material and thickness of each component were determined for the new model which was again verified by the random and fixed-frequency vibration analysis. The numerical results show that the final selection

Table 9. Stress of components.

Component	Material	Thick-ness (mm)	Maximum stress (MPa)	
			Random vibration	Fixed-frequency vibration
Upper bracket	980 DP	1.4	231.5	435.6
Lifting ear	780 DP	2.3	148.8	280.2
Bottom shell	780 DP	0.8	119.2	326.8
Lower support crossbeam	780 DP	1.3	149.6	146.9
Crossbeam	780 DP	1.6	60.8	193.8
Connecting bracket	B340	2.5	34	84.3
Short bracket	780 DP	1.5	69.3	156.3
Long bracket	780 DP	1.8	126.8	343.7
Lower support stringer	780 DP	1.5	94.9	461.4
Stringer	B210	1.8	88.2	198.4

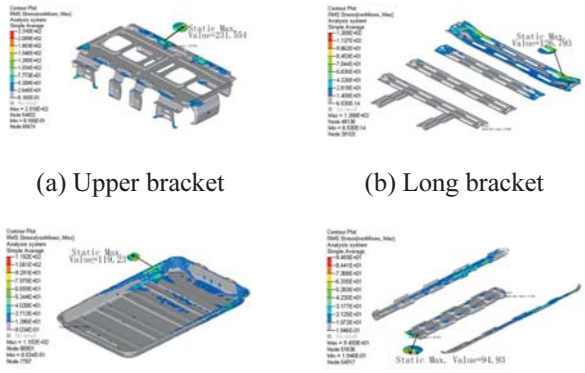

(a) Upper bracket (b) Long bracket

(c) Bottom shell (d) Stringer

Figure 5. Contour plot of stress in random vibration.

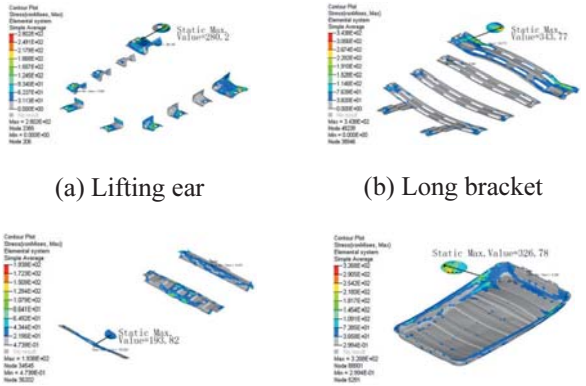

(a) Lifting ear (b) Long bracket

(c) Cross beam (d) Bottom shell

Figure 6. Contour plot of stress in fixed-frequency vibration.

of materials and thickness met the random and fixed-frequency vibration requirements. The stress of the main components are shown in Table 9, and the contour plot of stress is shown in Figures 5 and 6.

4.2. Fatigue Life Analysis

The BPE experiences a time-varying complex load because of the large-scale spatial movement during the actual driving period. In addition to meet higher strength and stiffness requirements, it also needs to have a long life cycle. Therefore, fatigue life analysis is important for the BPE to ensure the vehicle safety (Zhao *et al.*, 2014).

Fatigue life analysis was performed by the frequency domain method, counting the load information from the perspective of probability statistics and using PSD to describe the statistical characteristics of random vibration loads. It has advantages of simple idea and less calculation (Yang *et al.*, 2019). Figure 7 shows the flowchart of the random vibration fatigue life analysis.

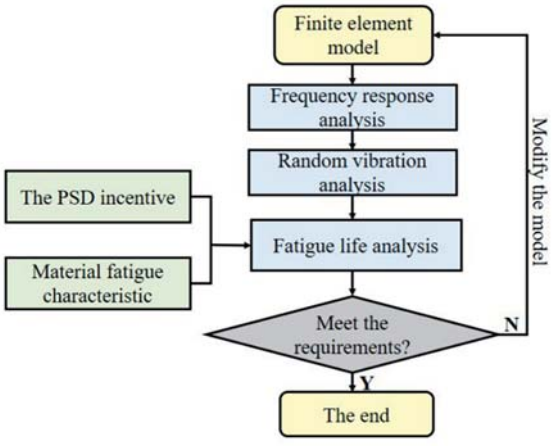

Figure 7. Flow chart of fatigue life analysis.

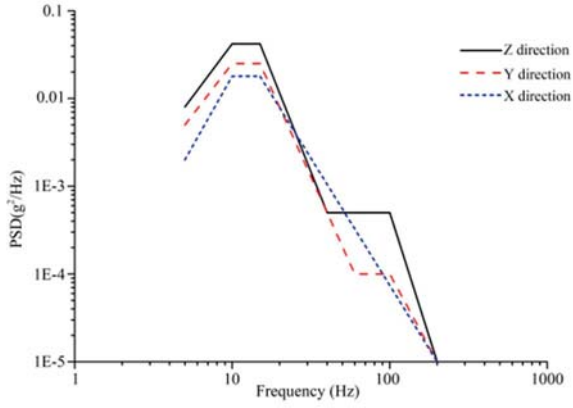

Figure 8. PSD curve for fatigue life analysis.

The frequency response was analyzed in advance to obtain the response of the BPE under a unit acceleration load, i.e., the transfer function. By introducing PSD excitation and material fatigue characteristic curve, the obtained results were subjected to random vibration fatigue analysis to predict the fatigue life. The PSD curve is shown in Figure 8. According to random vibration equivalent fatigue accelerated strengthening theory, a comprehensive PSD spectrum was obtained for the fatigue analysis by normalizing the road surface with the largest RMS value of

Table 10. Fatigue life of components.

Component	Material	Thickness (mm)	Fatigue life (s)
Upper bracket	980 DP	1.4	$\geq 2.2\times10^{6}$
Lifting ear	780 DP	2.3	$\geq 3.3\times10^{6}$
Bottom shell	780 DP	0.8	$\geq 4.04\times10^{8}$
Lower support crossbeam	780 DP	1.3	$\geq 3.4\times10^{6}$
Crossbeam	780 DP	1.6	$\geq 1.0\times10^{30}$
Short bracket	780 DP	1.5	$\geq 1.0\times10^{30}$
Long bracket	780 DP	1.8	$\geq 5.4\times10^{7}$
Lower support stringer	780 DP	1.5	$\geq 4.4\times10^{9}$

(a) Upper bracket

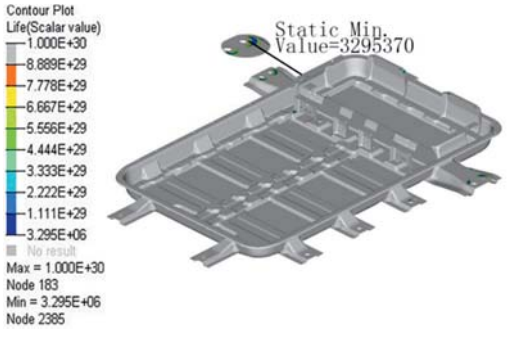

(b) Bottom shell

Figure 9. Fatigue life cloud diagrams.

vibration energy for various road surfaces. The target test time (12 h) is based on a harsh acceleration factor of 5, used to simulate the real world conditions requiring decreased test time and cost (Ministry of Industry and Information Technology of the People's Republic of China, 2020). The fatigue life of the main components is described in Table 10 and Figure 9.

The minimum fatigue life of the BPE is 2.2E+06 s, which is much longer than the 12 h (4.32E+04 s) required by the test standard. Thus, the possibility of the enclosure fatigue damage is quite small.

4.3. Mechanical Shock Analysis

Mechanical shock occurs frequently when the BPE is subjected to a sudden and aperiodic excitation. The goal of the mechanical shock analysis is to evaluate whether the BPE fails when it is subjected to a series of shocks. The magnitude of the mechanical shock varies greatly with complexity, and thus it is necessary to determine weak points of the structures and assess the integrity of the structure (Brand *et al.*, 2015). According to the "General Requirement of Traction Battery System for Electric Vehicles", a half sine wave shock was assumed and applied. The acceleration is 7 g, and the impact time is 6 ms, the range of the shock wave is shown in Figure 10. For taking account of the worse cases, the most stringent curve (E-F-G-H) was loaded in numerical analysis. The interval between two consecutive impacts should not be less than the response caused by the shocks on the BPE. Therefore, if the maximum stress of a impact cycle does not exceed the yield strength of the material, only one cycle mechanical shock simulation should be required.

The mechanical shock simulation was performed based on the FE model imposing the shock wave. The maximum stress values of each component are shown in Table 11.

The results show that the overall structural stress of the BPE does not exceed the yield strength of the material. Figure 11 shows the contour plot of stress in mechanical shock analysis.

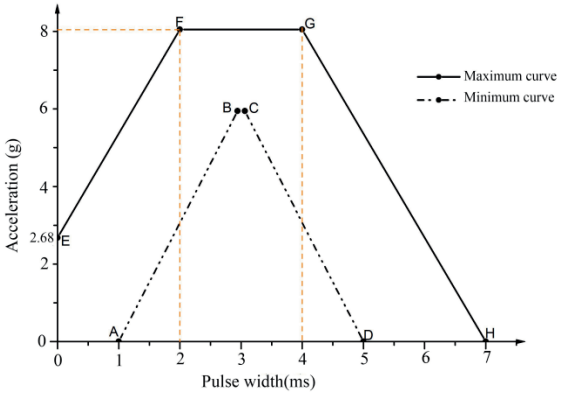

Figure 10. One cycle shock wave.

Table 11. Maximum stress of the components.

Component	Material	Thickness (mm)	Maximum stress (MPa)
Upper bracket	980 DP	1.4	280
Lifting ear	780 DP	2.3	434.8
Bottom shell	780 DP	0.8	256.9
Lower support crossbeam	780 DP	1.3	270.3
Crossbeam	780 DP	1.6	179.3
Connecting bracket	B340	2.5	53.9
Short bracket	780 DP	1.5	309.4
Long bracket	780 DP	1.8	235.6
Lower support stringer	780 DP	1.5	340.8

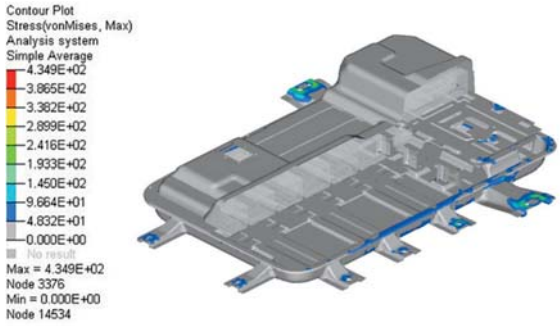

Figure 11. Contour plot of stress in mechanical shock.

The maximum stress is 434.8 MPa, occurring on the lifting ear. The optimized BPE met the requirements of mechanical shocks.

5. CRASH AND CRUSH SIMULATIONS

The automotive BPE was particularly subjected to high stress and large deformation in crash and crush conditions, posing safety issues such as explosions and fires. The vehicle safety has always been a major factor hindering the development of electric vehicles, thus performing crashworthiness analysis for the BPE is critical (Chen *et al.*, 2019; Diermann and Middendorf, 2019; Kukreja *et al.*, 2016). In this section, the crashworthiness was numerically analyzed in terms of crash and crush simulations.

The stress–strain curves are shown in Figure 12, determined by the Johnson–Cook constitutive model. This is the most common, yet simplest model to describe both high stress and the high strain rates of materials, as a result of increasing temperature. The crashworthiness was

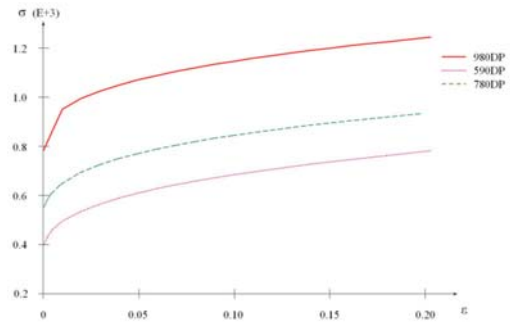

Figure 12. Material constitutive model.

investigated using the governing equations and explicit FE code LS-DYNA at both component and vehicle levels. In the hourglass control, the stiffness form by Flanagan-Belytschko, with exact volume integration, was considered, keeping hourglass coefficient as 0.1. This coefficient will lead to numerical instability effects if it exceeds 0.15. When the contact type was set, a penalty coefficient was used. The value 0.1 was selected for sliding interface penalties (SLSFAC). A value of 1.0 was recommended for rigid wall penalties, where rigid bodies interact with fixed rigid walls (RWPNAL).

5.1. Crash Simulation

To evaluate the mechanical damage caused by electric vehicle collision accidents and ensure the collision safety of battery packs, the crash simulation of the optimized BPE was performed. The crash simulation needs to be performed in both X- and Y-axis directions. The relevant loading parameters are shown in Figure 13 according to the test standard.

Setting a suitable time step is critical to perform the crash simulation. If the time step is small, the simulation time will increase significantly. In contrast, if the time step is large, the crash simulation may be unstable, sharply decreasing the accuracy. In general, the maximum stable step time of the FE model can be approximately described as:

$$\Delta t = \frac{L}{c} = L\sqrt{\frac{\rho}{E}} \tag{6}$$

where L represents the length of the FE, and ρ and E are the mass density and elastic modulus, respectively.

By implementing the crash simulation, the stress and strain of the BPE components are listed in Table 12. The overall contour plot of stress are shown in Figure 14.

The results show that the maximum stress in X-axis crash occurs on the bottom shell with a value of 828.7 MPa. Although it exceeds the yield strength of the material, it does not exceed the tensile strength of the material and the related strain is very small. The maximum stress in Y-axis crash is 524.1 MPa, which does not exceed the yield strength of the material. Therefore, the optimized BPE met the crash requirements.

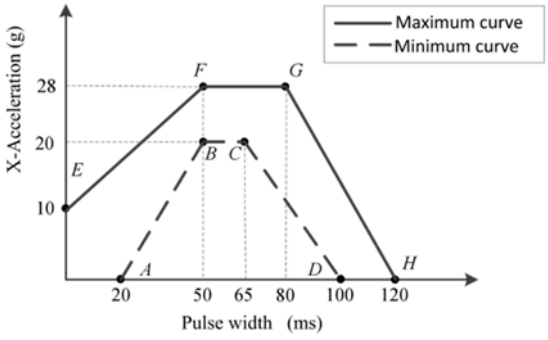

(a) X-axis

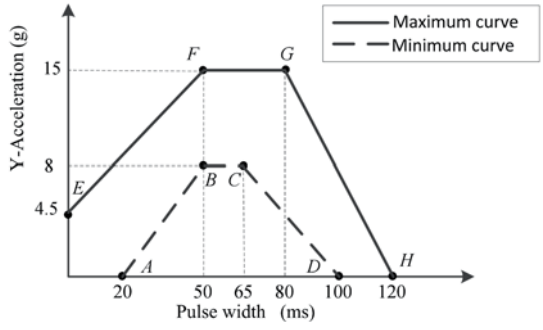

(b) Y-axis

Figure 13. Parameters of crash simulation.

Table 12. Stress and strain of components.

Component	Material	Stress (MPa)		Corresponding strain	
		X-axis	Y-axis	X-axis	Y-axis
Upper bracket	980 DP	609.6	524.1	0.0072	0
Lifting ear	780 DP	685	380.3	0.0011	0
Bottom shell	780 DP	828.7	493.6	0.00483	0
Lower support crossbeam	780 DP	689.5	360.6	0.00141	0
Crossbeam	780 DP	628.4	287	0.00007	0
Connecting bracket	B340	157.3	141.5	0	0
Short bracket	780 DP	313.7	367.2	0	0
Long bracket	780 DP	498.1	362.4	0	0
Lower support stringer	780 DP	601.9	199.9	0.00001	0
Stringer	B210	356.2	340.2	0.00947	0.00243

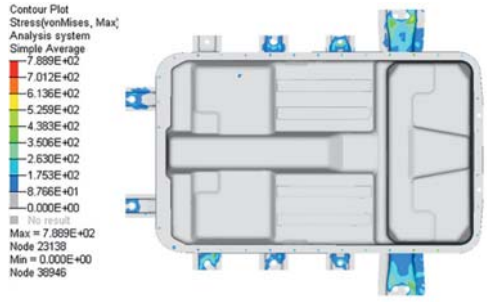

(a) X-axis

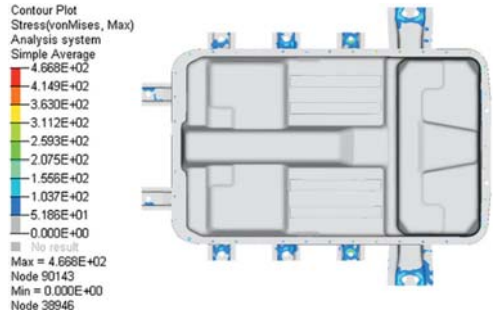

(b) Y-axis

Figure 14. Contour plot of stress in crash simulation.

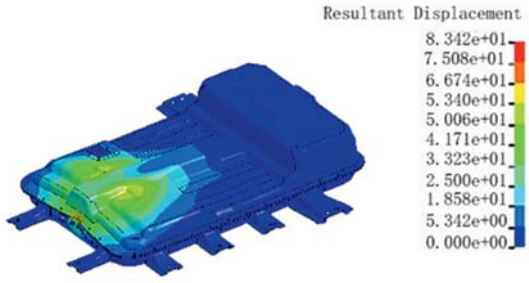

(a) X-axis

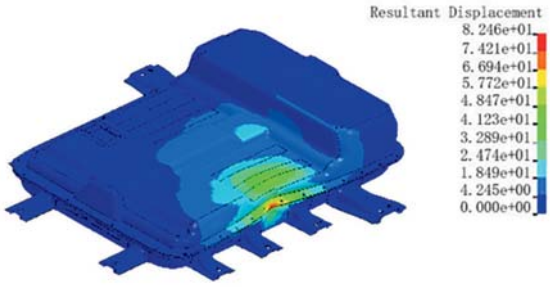

(b) Y-axis

Figure 16. Contour plot of stress in crush simulation.

5.2. Crush Simulation

The applied crush force emulates a vehicle accident or any external force that may damage the battery packs, resulting in high stress and large deformation. The crush test is also referred to as the battery enclosure integrity test, which needs to be performed separately in both X- and Y-axis directions. The extrusion speed is 2 mms^{-1} according to the test standard. In order to shorten the simulation time, the extrusion speed is usually set to 2 ms^{-1} based on experiences. The crush simulation stops when the extrusion plate reaches 100 kN or the extrusion deformation of the battery-pack shell reaches 30 %. The extruded plate is shown in Figure 15.

Figure 16 show the results of the crush analysis. In X-axis direction, when the extrusion plate reaches 100 kN, the battery-pack case has not yet touched the module, thus the module will not be in danger such as leakage and explosion. In Y-axis direction, when the extrusion plate reaches 100 kN, the battery-pack case slightly squeezes to the module, but the stress value (about 62 MPa) is small, thus it will not cause any damage to the module. As a result, the optimized model met the crush requirements as well.

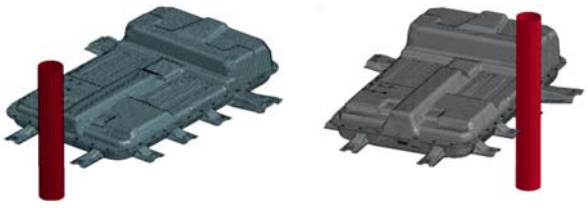

(a) X-axis (b) Y-axis

Figure 15. Crush simulation.

6. CONCLUSIONS

In conclusion, a nonlinear FE model was established based on the detailed structure of a BPE. The modal analysis and bench test were applied to verify the effectiveness of the FE model. Whether the verified model can be applied to highly non-linear fields such as crashworthiness still requires bench tests. The material and thickness were primarily selected based on the random vibration analysis. The final material and thickness selection was determined by fixed-frequency vibration, mechanical shock, and fatigue life analysis. The crashworthiness performance of the optimized BPE was evaluated in terms of crush and crash simulations. The results show that the optimized enclosure met the requirements of vibration, mechanical shock, and crashworthiness and reduced the total weight by 10.41 %.

Because of the time consuming and expensive experimental methods, the presented numerical method based on AHSSs and size optimization has some theoretical and practical significance. The presented result is not the only optimized solution, it belongs to the Parato solution set. The resulting Parato solution set will change with the

change in the structure of the BPE and the lightweight design process. However, the analysis procedure can still be used to guide engineering practice, reduce the number of tests and product development costs, and shorten product development cycles.

ACKNOWLEDGEMENT–This study was funded by the National Natural Science Foundation of China (Project No.12072050) and the Fundamental Research Funds for the Central Universities (Project No.2021CDJQY-032).

REFERENCES

Arora, S., Shen, W. and Kapoor, A. (2016). Review of mechanical design and strategic placement technique of a robust battery pack for electric vehicles. *Renewable and Sustainable Energy Reviews*, **60**, 1319–1331.

Brand, M. J., Schuster, S. F., Bach, T., Fleder, E., Stelz, M., Gläser, S., Müller, J., Sextl, G. and Jossen, A. (2015). Effects of vibrations and shocks on lithium-ion cells. *J. Power Sources*, **288**, 62–69.

Chen, C., Xiong, F. C., Lan, F. and Kuang, S. S. (2019). Crush simulation and optimisation study of power battery pack. *Int. J. Vehicle Safety* **11**, **1**, 37–55.

Chen, L. and X. Y. Zhao. (2019). Lightweight design and static strength analysis of battery box for electric vehicle. *Proc. 2019 Int. Conf. Robotics, Intelligent Control and Artificial Intelligence, Association for Computing Machinery*. Shanghai, China.

Chen, X., Li, M., Li, S., Jin, J. and Zhang, C. (2017a). Design optimization of multi-material battery enclosure for electric vehicle. *Society of Automotive Engineers (SAE)-China Cong*., Singapore, Singapore.

Chen, Y., Liu, G., Zhang, Z. Y. and Hou, S. J. (2017b). Integrated design technique for materials and structures of vehicle body under crash safety considerations. *Structural and Multidisciplinary Optimization* **56**, **2**, 455 –472.

Diermann, V. and P. Middendorf. (2019). Automatic evaluation of structural integrity in crashworthiness simulations using image analysis. *Int. J. Automotive Technology* **20**, **1**, 65–72.

Hartmann, M., Roschitz, M. and Khalil, Z. (2013). Enhanced battery pack for electric vehicle: Noise reduction and increased stiffness. *Materials Science Forum*, **765**, 818–822.

Hong, S. K., Epureanu, B. I. and Castanier, M. P. (2014). Parametric reduced-order models of battery pack vibration including structural variation and prestress effects. *J. Power Sources*, **261**, 101–111.

Kaleg, S. (2016). 1P15S lithium battery pack: Aluminum 5052-0 strength of material analysis and optimization. *Int. Conf. Sustainable Energy Engineering and Application (ICSEEA), IEEE*. Tangerang, Banten, Indonesia.

Kukreja, J., Nguyen, T., Siegmund, T., Chen, W., Tsutsui, W., Balakrishnan, K., Liao, H. and Parab, N. (2016). Crash analysis of a conceptual electric vehicle with a damage tolerant battery pack. *Extreme Mechanics Letters* **9**, **3**, 371–378.

Lang, J. F. and Kjell, G. (2015). Comparing vibration measurements in an electric vehicle with standard vibration requirements for li-ion batteries using power spectral density analysis. *Int. J. Electric and Hybrid Vehicles* **7**, **3**, 272–286.

Li, W., Xia, Y., Chen, G. H. and Sahraei, E. (2018). Comparative study of mechanical-electrical thermal responses of pouch, cylindrical, and prismatic lithium-ion cells under mechanical abuse. *Science China Technological Sciences* **61**, **10**, 1472–1482.

Lin, C., Gao, F. L., Wang, W. W., and Chen, X. K. (2016). Multi-objective optimization design for a battery pack of electric vehicle with surrogate models. *J. Vibroengineering* **18**, **4**, 2343–2358.

Liu, Z., Lu, J. H. and Zhu, P. (2016). Lightweight design of automotive composite bumper system using modified particle swarm optimizer. *Composite Structures*, **140**, 630–643.

Liu, Z., Li, H., & Zhu, P. (2019). Diversity enhanced particle swarm optimization algorithm and its application in vehicle lightweight design. *J. Mechanical Science and Technology* **33**, **2**, 695–709.

Obradovic, J., Boria, S. and Belingardi, G. (2012). Lightweight design and crash analysis of composite frontal impact energy absorbing structures. *Composite Structures* **94**, **2**, 423–430.

Pal, S. K., Singh, S., Singh, H., Le Phung, M. L., Yooyen, S. and Sleesongsom, S. (2020). Intelligent design optimization of battery pack enclosure for electric vehicle by considering cold-spraying as an additive manufacturing technology. *Energy Storage* **2**, **3**. e148.

Schludi, C. and Joos, J. (2019). Lightweight and safe composite battery housings. *Lightweight Design Worldwide* **12**, **6**, 44–47.

Uerlich, R., Sanalkumar, K. A., Bokelmann, T. and Vietor, T. (2020). Finite element analysis considering packaging efficiency of innovative battery pack designs. *Int. J. Crashworthiness* **25**, **6**, 664–679.

Wang, L., Chen, X. K. and Zhao, Q. H. (2016). Muti-objective topology optimization of an electric vehicle's traction battery enclosure. *Energy Procedia*, **88**, 874–880.

Yang, G. X., Wang, M., Li, Q. and Ding, R. (2019). Methodology to evaluate fatigue damage of high-speed train welded bogie frames based on on-track dynamic stress test data. *Chinese J. Mechanical Engineering* **32**, **1**, 1–8.

Zhao, N. Z., Li, W., Cai, W. W. and Abell, J. A. (2014). A fatigue life study of ultrasonically welded lithium-ion battery tab joints based on electrical resistance. *J. Manufacturing Science and Engineering* **136**, **5**, 051003.

Zienkiewicz, O. C., Taylor, R. L. and Fox, D. (2014). *The Finite Element Method for Solid and Structural Mechanics*. Elsevier. Amsterdam, Netherlands.